Monthly Notices
of the
ROYAL ASTRONOMICAL SOCIETY

MNRAS **481,** 566–577 (2018)
Advance Access publication 2018 August 23

doi:10.1093/mnras/sty2291

The impact of spiral density waves on the distribution of supernovae

A. G. Karapetyan,[1⋆] A. A. Hakobyan,[1⋆] L. V. Barkhudaryan,[1] G. A. Mamon,[2] D. Kunth,[2] V. Adibekyan[3] and M. Turatto[4]

[1]*Byurakan Astrophysical Observatory, 0213 Byurakan, Aragatsotn province, Armenia*
[2]*Institut d'Astrophysique de Paris, Sorbonne Universités, UPMC Univ Paris 6 et CNRS, UMR 7095, 98 bis bd Arago, F-75014 Paris, France*
[3]*Instituto de Astrofísica e Ciência do Espaço, Universidade do Porto, CAUP, Rua das Estrelas, P-4150-762 Porto, Portugal*
[4]*INAF – Osservatorio Astronomico di Padova, Vicolo dell'Osservatorio 5, I-35122 Padova, Italy*

Accepted 2018 August 18. Received 2018 August 9; in original form 2018 June 26

ABSTRACT

We present an analysis of the impact of spiral density waves (DWs) on the radial and surface density distributions of supernovae (SNe) in host galaxies with different arm classes. We use a well-defined sample of 269 relatively nearby, low-inclination, morphologically non-disturbed and unbarred Sa–Sc galaxies from the Sloan Digital Sky Survey, hosting 333 SNe. Only for core-collapse (CC) SNe, a significant difference appears when comparing their R_{25}-normalized radial distributions in long-armed grand-design (LGD) versus non-GD (NGD) hosts, with that in LGD galaxies being marginally inconsistent with an exponential profile, while SNe Ia exhibit exponential surface density profiles regardless of the arm class. Using a smaller sample of LGD galaxies with estimated corotation radii (R_C), we show that the R_C-normalized surface density distribution of CC SNe indicates a dip at corotation. Although not statistically significant, the high CC SNe surface density just inside and outside corotation may be the sign of triggered massive star formation by the DWs. Our results may, if confirmed with larger samples, support the large-scale shock scenario induced by spiral DWs in LGD galaxies, which predicts a higher star formation efficiency around the shock fronts, avoiding the corotation region.

Key words: supernovae: general – galaxies: kinematics and dynamics – galaxies: spiral – galaxies: star formation – galaxies: structure.

1 INTRODUCTION

The spiral arm structure of star-forming disc galaxies was explained in the framework of density wave (DW) theory by the pioneering work of Lin & Shu (1964). According to this theory, semi-permanent spiral patterns especially in grand-design (GD) galaxies, i.e. spiral galaxies with prominent and well-defined spiral arms, are created by long-lived quasi-stationary DWs. Despite an excellent progress of the theory (for recent comprehensive reviews, see Dobbs & Baba 2014; Shu 2016), there are many disputes on the lifetime of spiral patterns, and the ability of DWs to generate large-scale shocks and trigger star formation, as originally proposed by Roberts (1969). For example, the simulations by Sellwood (2011) manifest short-lived patterns. In another example, using a multiband analysis for some GD galaxies, Foyle et al. (2010) found that there is no shock trigger, and that the spiral arms just reorganize the material from the disc out of which stars form (see also Grosbøl & Dottori 2012).

Nevertheless, the results of many other studies are consistent with the picture where the DWs cause massive star formation to occur by compressing gas clouds as they pass through the spiral arms of GD galaxies (e.g. Cepa & Beckman 1990; Knapen et al. 1996; Seigar & James 2002; Grosbøl & Dottori 2009; Martínez-García, González-López lira & Bruzual-A 2009). For example, using Hα direct imaging accompanied with broad-band images in R and I bands, Cedrés et al. (2013) studied the distribution of H II regions of spiral arms and found clear evidence for the triggering of star formation in the sense of a high density of H II regions at the fixed radial ranges in some GD galaxies. Recently, Pour-Imani et al. (2016) showed that pitch angle of galaxies is statistically more tightly wound, i.e. smaller, when viewed in the light from the evolved/older stellar populations. Both the results, complementing each other, are in excellent agreement with the prediction of theory that stars are not only born in the DW but also move out of it as they age (see also most recent results by Shabani et al. 2018).

An alternative to the DW theory is the idea of reorganization of the distribution of H II regions in multiple arms of differentially rotating disc with star formation processes generated by the stochastic self-propagating method developed by Mueller & Arnett (1976) and

⋆ E-mail: karapetyan@bao.sci.am (AGK); hakobyan@bao.sci.am (AAH)

Gerola & Seiden (1978). This mechanism is supposed to work in non-GD (NGD) galaxies, producing flocculent spiral arms.

In the context of above-mentioned scenarios, the main goal of this article is to study the possible impact of spiral DWs (triggering effect) on the distribution of supernovae (SNe) in discs of host galaxies, when viewing in the light of different nature of Type Ia and core-collapse (CC) SNe progenitors. Recall that Type Ia SNe result from stars with masses lower than $\sim$7.5 $M_\odot$ (ages from $\sim$0.5 Gyr up to $\sim$10 Gyr, see Maoz & Mannucci 2012) in close binary systems, while the progenitors of Types Ibc and II SNe,[1] collectively called CC SNe, are massive ($M \gtrsim 7.5\,M_\odot$, see e.g. Williams et al. 2018) young short-lived stars (from a few up to $\sim$100 Myr, see Anderson et al. 2015; Maund 2018; Xiao et al. 2018).

The first attempt to study the distribution of SNe within the framework of DW theory was performed by Moore (1973). Using the locations of 19 SNe, he suggested that stars in a spiral galaxy are formed in a shock front on the inner edge of a spiral arm, then drift across the arm as they age, predicting for SN progenitors (more likely for SNe II) a short lifetime (a few million years) and high masses (a few tens of solar masses). However, using the fractions of GD and flocculent galaxies in a sample of 111 hosts with 144 SNe, McCall & Schmidt (1986) suggested that DWs do not greatly enhance the massive star formation rate per unit luminosity of a galaxy, mentioning that star formation in most galaxies may be dominated by stochastic processes. Results similar to those in Moore (1973) were obtained also by McMillan & Ciardullo (1996) and Mikhailova, Bartunov & Tsvetkov (2007) for Types II and Ibc SNe, respectively. In other studies, different authors (e.g. Maza & van den Bergh 1976; Bartunov, Tsvetkov & Filimonova 1994; Petrosian et al. 2005) investigated the distribution of SNe relative to spiral arms of galaxies. Such studies did not interpret their results within the DW theory nor did they distinguish among various spiral arm classes (ACs; Elmegreen & Elmegreen 1987) of SNe host galaxies.

Indeed, in our recent paper (Aramyan et al. 2016), we already studied the distribution of SNe relative to the spiral arms of their GD and NGD host galaxies, using the Sloan Digital Sky Survey (SDSS) images from the *g*, *r*, and *i* bands. We found that the distribution of CC SNe (i.e. tracers of recent star formation) is affected by the spiral DWs in their host GD galaxies, being distributed closer to the corresponding edges of spiral arms where large-scale shocks, thus star formation triggering, are expected (see also farther in the text of Section 4). Such an effect was not observed for Type Ia SNe (less-massive and longer-lived progenitors) in GD galaxies, as well as for both types of SNe in NGD hosts. In this paper, we expand our previous work, and for the first time study the differences between the radial distributions of SNe in unbarred Sa–Sc host galaxies with various spiral ACs. In parallel, to check the triggering effect at different galactocentric radii, we study the consistency of the surface density distribution of SNe (normalized to the optical radii, and for a smaller sample also to corotation radii of hosts) with an exponential profile in GD and NGD galaxies.

The layout of this article is the following. In Section 2, we present sample selection and reduction, and determination approach of spiral ACs. The results and their interpretation within the framework of DW theory are presented in Sections 3 and 4, respectively. Section 5 summarizes our conclusions. To conform to the values used in databases of our recent papers (Hakobyan et al. 2012, 2014, 2016; Aramyan et al. 2016), a cosmological model with $\Omega_m = 0.27$, $\Omega_\Lambda = 0.73$, and $H_0 = 73\,km\,s^{-1}\,Mpc^{-1}$ Hubble constant (Spergel et al. 2007) are adopted in this article.

2 THE SAMPLE

In order to obtain a homogeneous data set of structural features of SNe host galaxies, including morphology, and identification of bars and spiral ACs, we compile the sample of this study in the same way as in Hakobyan et al. (2012), being restricted to relatively nearby SNe with distances $\leq$150 Mpc. The whole compilation, reduction, and classification procedures are given below.

2.1 Sample selection and reduction

We used the updated version of the Asiago Supernovae Catalogue (ASC; Barbon et al. 1999), which at the time of writing the article includes SNe detected before 1 July 2017. To identify SNe host galaxies, we cross-matched the coordinates of all classified Type Ia and CC (Ibc and II) SNe from the ASC with the footprint of the SDSS Data Release 13 (DR13; Albareti et al. 2017). We then classified the identified host galaxies according to Hakobyan et al. (2012) and selected only Sa–Sc types,[2] since it is known that both GD and NGD shapes are well represented in Sa–Sc spirals (e.g. Ann & Lee 2013; Bittner et al. 2017).

We excluded all barred galaxies from our sample to eliminate the effect of substantial suppression of massive star formation in the radial range swept by strong bars (e.g. James, Bretherton & Knapen 2009; James & Percival 2018), i.e. the observed suppression of CC SN numbers inside the bar radius (Hakobyan et al. 2016), and study only the expected impact of the DWs on the distribution of SNe.[3] In addition, we removed host galaxies with strong morphological disturbances according to Hakobyan et al. (2014), i.e. interacting, merging, and post-merging/remnant cases, which may add significant distortion into the SN distribution in discs of galaxies.

For the remaining SNe host galaxies, the next step is the measurement of their photometry and geometry. Following Hakobyan et al. (2012), we constructed 25 mag arcsec^{-2} isophotes in the SDSS DR13 *g*-band, and then visually fit onto each isophote an elliptical aperture. We then measured the major axes (D_{25}), elongations (a/b), and position angles (PA) of galaxies. In our analysis, we used the D_{25} corrected for Galactic (Schlegel, Finkbeiner & Davis 1998) and host galaxy internal extinction (Bottinelli et al. 1995). Finally, we calculated the inclinations of host galaxies using elongations and morphological types, following the method presented in Paturel et al. (1997). These procedures are explained in detail in Hakobyan et al. (2012).

We also removed highly inclined galaxies ($i > 60^\circ$), because at these inclinations strong absorption and projection effects play a destructive role in discovering SNe (e.g. Cappellaro & Turatto

[1]Traditionally, SNe of Types Ib and Ic, including uncertain spectroscopic Type Ib/c, are denoted as SNe Ibc. All these and other subtypes of CC SNe, i.e. Ibc, II, IIb (transitional objects with observed properties close to SNe II and Ib), and IIn (dominated by emission lines with narrow components) SNe, arise from young massive stars with possible differences in their masses, metallicities, and ages (see e.g. Smith et al. 2011, for more details).

[2]Many of the identified host galaxies are already listed in database of Hakobyan et al. (2012), which is based on the SDSS DR8. Here, because we added new SNe, for homogeneity we redid the entire reduction for this restricted sample based only on DR13.

[3]It is important to note that in some SN host galaxies we may not detect tiny bars with lengths shorter than a tenth of the optical disc (Hakobyan et al. 2014). However, by the inner truncation of host discs (see SubSection 3.1) we exclude any possible impact of these bars on the distribution of SNe.

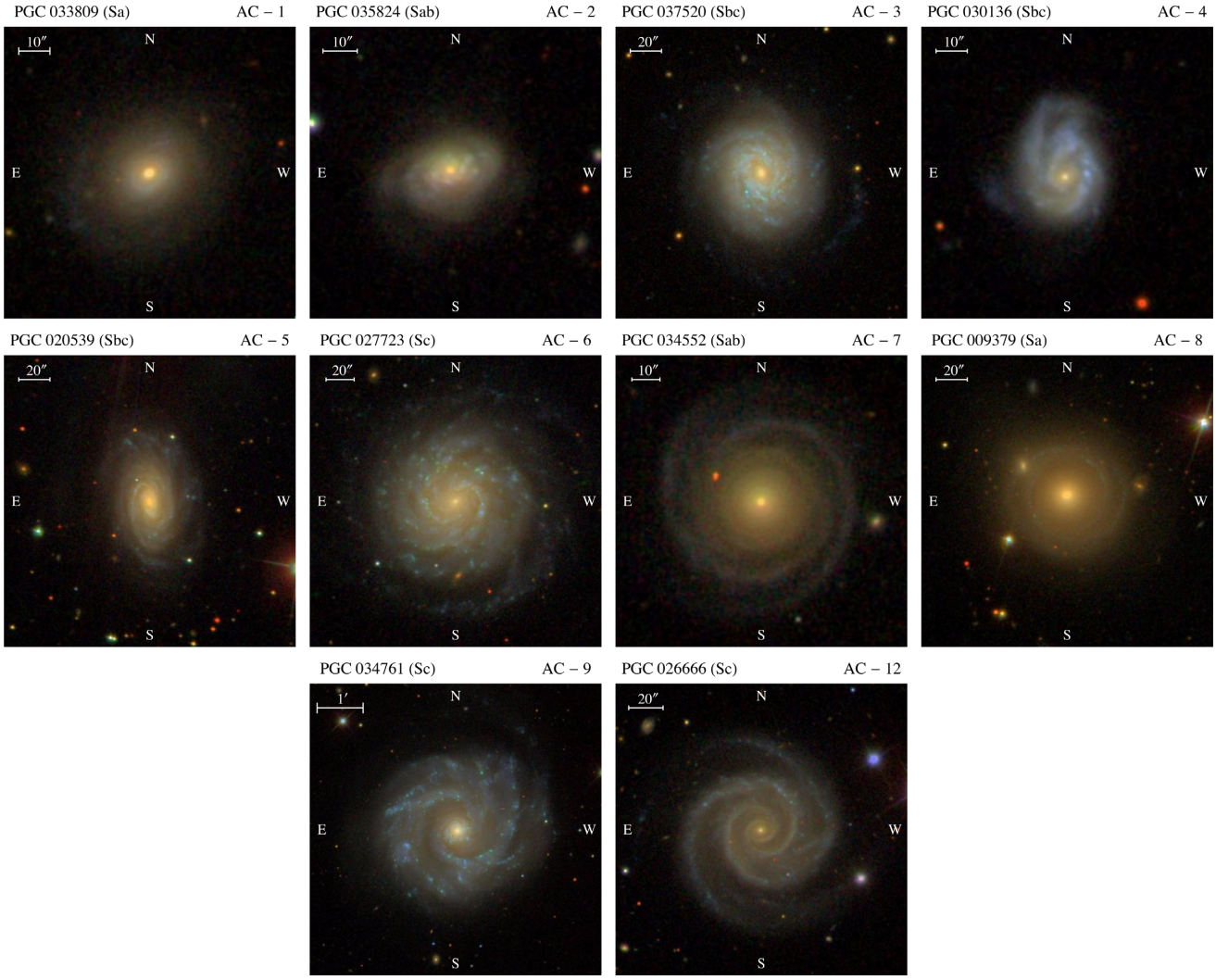

Figure 1. SDSS images representing examples of unbarred Sa–Sc host galaxies with different arm classes (ACs) according to Elmegreen & Elmegreen (1987). The Principal Galaxy Catalogue (PGC) objects' identifiers, morphological types (in parentheses), and ACs are listed at the top. In all images, north is up and east is to the left.

1997) and correcting their radial distribution for inclination of host disc (e.g. Hakobyan et al. 2016). Moreover, it is difficult to classify highly inclined galaxies and determine their barred structure (see review by Buta 2013).

After these operations, we obtained 353 SNe within 285 host galaxies with the aforementioned restrictions.

2.2 Determination of spiral arm classes

Following our recent study (Aramyan et al. 2016), we determined ACs of 285 host galaxies (unbarred Sa–Sc types) with $i \leq 60^{\circ}$ according to the classification scheme by Elmegreen & Elmegreen (1987). To accomplish this, we used the background subtracted and photometrically calibrated g-band[4] SDSS images, as well as the RGB colour images from the g, r, and i SDSS data channels. We assigned ACs according to the flocculence, regularity, and shapes of the spiral arms. The SDSS three-colour images representing examples of SN host galaxies with different ACs can be found in Fig. 1. Below, we describe these classes in detail according to Elmegreen & Elmegreen (1987).

Galaxies with AC 12 contain two long symmetric arms, and the ones with AC 9 have two symmetric inner arms, multiple long and continuous outer arms. The underlying mechanism that explains the lengths of arms and their global symmetry in these galaxies is most probably a DW, dominating the entire optical disc (e.g. Elmegreen, Elmegreen & Montenegro 1992). We denote galaxies with ACs 9 and 12 as long-armed GD (LGD) galaxies.

Galaxies with AC 5 have two symmetric short arms in the inner region and irregular outer arms. The AC 6 is like AC 5 in the inner disc region, however with feathery ring-like outer structure. The short inner symmetric arms in these galaxies might be explained by the DW mechanism, dominating only in the inner part of the optical disc (e.g. Elmegreen et al. 1992). We denote galaxies with ACs 5 and 6 as short-armed GD (SGD) galaxies.

Galaxies with AC 1 are described by chaotic, fragmented, and unsymmetric arms, AC 2 is fragmented spirals arm pieces with no regular pattern, AC 3 is fragmented arms uniformly distributed

[4]Among the SDSS g, r, and i bands with good signal-to-noise ratio, the arm–interarm contrast is the highest in the g-band, as it traces the young stellar populations in the spiral arms (see Aramyan et al. 2016).

Table 1. Numbers of SNe at distances ≤ 150 Mpc in unbarred Sa–Sc hosts with inclinations $i \leq 60^{\circ}$, split between LGD, SGD, and NGD galaxies.

	Sa	Sab	Sb	Sbc	Sc	All
			LGD (9, 12)			
Ia	2	4	7	21	27	61
Ibc	1	0	2	14	19	36
II	0	1	13	22	61	97
All	3	5	22	57	107	194
			SGD (5, 6)			
Ia	0	0	2	8	8	18
Ibc	0	0	2	1	6	9
II	0	0	3	7	22	32
All	0	0	7	16	36	59
			NGD (1-4)			
Ia	3	3	5	10	11	32
Ibc	0	5	1	4	4	14
II	1	1	4	9	19	34
All	4	9	10	23	34	80

Notes. Among these 333 SNe, there are only 23 uncertain (20 peculiar) classifications. SNe of Type II include only 10 SNe IIb. All Type IIn SNe are removed from the sample due to uncertainties in their progenitor nature (e.g. Habergham et al. 2014), and often in their classification (e.g. Silverman et al. 2013; Pastorello et al. 2018).

around the galactic centre. Galaxies with AC 4 have only one permanent arm, otherwise fragmented arms. All these flocculent galaxies (ACs 1–4) appear to lack global DWs, instead their spirals may be sheared self-propagating star formation regions (see review by Buta 2013, and references therein). We denote galaxies with ACs 1–4 as NGD galaxies.

Galaxies with AC 7 have two symmetric long outer arms, feathery or irregular inner arms. In these galaxies, the DWs play a role, most probably, only in the outer part of the optical disc (see review by Buta 2013, and references therein). In our study, due to the small number statistics (especially for CC SNe), these galaxies are not denoted to a separate class. We have only 11 Type Ia and 6 CC SNe in these hosts. On the other hand, because of the different placement of DWs, it is inadvisable to mix them with other classes. Therefore, we simply omit them from the sample.

Galaxies with AC 8 have tightly wrapped ring-like arms. These ring-like arms (rings and pseudorings) are thought to be related to the gathering of material near dynamical resonances in the disc (see review by Buta 2013). Because of the different structural feature and small number statistics (only three Type Ia SNe), we omit these galaxies from the sample as well.

Finally, according to Elmegreen & Elmegreen (1987), ACs 10 and 11 were previously reported to be barred galaxies and objects with close neighbours, respectively, and are no longer used.

In the present study, we mainly used these broad classes: LGD (AC 9, 12), SGD (AC 5, 6), and NGD (AC 1-4). Table 1 presents the distributions of 333 SN types among various morphological types of the broad ACs of host galaxies. The number of individual host galaxies is 269. The mean distance of the galaxies is 82 Mpc (standard deviation is 39 Mpc). The mean D_{25} of the hosts is 120 arcsec with the minimum value of 23 arcsec. In Table 1, we present the numbers of Types Ibc and II SNe separately. However, to increase statistical significance of our results (especially in Section 4), we combined SNe Ibc and II into a single CC SNe class.

In order to test our visual classification of spiral arms, the entire sample of SNe host galaxies was independently classified by the first three authors of this paper. By comparing these classifications, we determined that our ACs are 97 per cent reliable. Following Aramyan et al. (2016), it is important to note that the most common mis-classifications of ACs are from 2 or 3 to 4 (or vice versa), from 5 to 6 (or vice versa), and from 9 to 12 (or vice versa). Because we separated SNe host galaxies by their ACs into three broad classes: LGD, SGD, and NGD, the possible mis-classification between them is negligible.

Of the sample galaxies, 56 are in common with galaxies for which ACs were determined by Elmegreen & Elmegreen (1987) on the blue images of the Palomar Observatory Sky Survey (POSS).[5] A comparison of the ACs shows that about 65 per cent of the galaxies have the same broad classes. On the other hand, about 25 per cent of objects change from NGD to SGD or from SGD to LGD (or vice versa). The ACs change from NGD to LGD (or vice versa) only in about 10 per cent of the cases (six individual galaxies). In all the cases, the SDSS images have deeper exposure and better resolution that the blue photographic plates of the POSS (in some cases, they are even overexposed due to high surface brightness of the object). Therefore, the SDSS-based arm-classification seems to be more reliable and more structure is revealed.

The full database of 333 individual SNe (SN designation, type, and offset from host galaxy nucleus) and their 269 hosts (galaxy SDSS designation,[6] distance, morphological type, *a*/*b*, PA, corrected *g*-band D_{25}, and AC) is available in the online version (Supporting Information) of this article.

3 RESULTS

To reveal the possible influence of DWs in discs of Sa–Sc galaxies on the distribution and surface density of SNe, we now study the deprojected and normalized galactocentric radii of Type Ia and CC SNe in discs of host galaxies with various ACs.

3.1 The radial distribution and surface density

In Hakobyan et al. (2016, 2017), we already showed that in spiral galaxies all CC SNe and the overwhelming majority of Type Ia SNe belong to the disc, rather than the bulge component. Considering this observational fact, we adopt a simplified model where all SNe are located on infinitely thin host discs and, following Hakobyan et al. (2009), we deproject the galactocentric radii of SNe ($R_{\rm SN}$) for the inclinations of these discs. For each SN, we then normalize $R_{\rm SN}$ to the corresponding host galaxy optical radius, i.e. $R_{25} = D_{25}/2$, to neutralize the greatly different linear (in kpc) sizes of various hosts (as was shown in Hakobyan et al. 2009).[7]

[5]For comparison of ACs, another arm-classification by Buta et al. (2015) might be used. However, it is based on middle-infrared images (while we use the SDSS/optical images) and another definition of broad ACs (flocculent: grouping 1–4 ACs, multi-arm: grouping 5–9 ACs, and GD: only AC 12), which complicate the comparison.

[6]For the host galaxies included in Table 4, the PGC names are also available in the database.

[7]For the normalization, one can suggest to use the SDSS scale lengths (exponential model fits) of galaxies. However, our sample includes a large number of host galaxies with large angular sizes (>100 arcsec) for which the SDSS fails in estimation of the model scale lengths due to the blending/defragmenting of galaxies with large angular sizes (the scales are not reliable, this is a well-known problem). In Hakobyan et al. (2012), we al-

Table 2. Comparison of the deprojected and normalized radial distributions of SNe ($\tilde{r} = R_{SN}/R_{25}$) among different pairs of NGD, SGD, and LGD subsamples. The corresponding values for the inner-truncated disc ($\tilde{r} \geq 0.2$) are listed in parentheses.

Subsample 1				Subsample 2				
Host	SN	N_{SN}		Host	SN	N_{SN}	P_{KS}	P_{AD}
LGD	Ia	61 (50)	versus	NGD	Ia	32 (24)	0.521 (0.497)	0.690 (0.708)
LGD	Ia	61 (50)	versus	SGD	Ia	18 (16)	0.761 (0.800)	0.505 (0.821)
NGD	Ia	32 (24)	versus	SGD	Ia	18 (16)	0.557 (0.641)	0.216 (0.671)
LGD	CC	133 (111)	versus	NGD	CC	48 (40)	0.087 (**0.048**)	0.106 (**0.022**)
LGD	CC	133 (111)	versus	SGD	CC	41 (39)	0.410 (0.096)	0.430 (0.125)
NGD	CC	48 (40)	versus	SGD	CC	41 (39)	0.080 (0.356)	0.108 (0.312)
LGD	Ia	61 (50)	versus	LGD	CC	133 (111)	0.720 (0.702)	0.719 (0.706)
SGD	Ia	18 (16)	versus	SGD	CC	41 (39)	0.834 (0.697)	0.862 (0.590)
NGD	Ia	32 (24)	versus	NGD	CC	48 (40)	0.545 (0.384)	0.284 (0.169)

Notes. The probabilities from two-sample KS and AD tests (P_{KS} and P_{AD}) are calculated using the calibrations by Massey (1951) and Pettitt (1976), respectively. The statistically significant differences between the distributions are highlighted in bold.

In Table 2, using the two-sample Kolmogorov–Smirnov (KS) and Anderson–Darling (AD) tests,[8] we compare the deprojected and normalized ($\tilde{r} = R_{SN}/R_{25}$) radial distributions of Type Ia and CC SNe in different pairs of NGD, SGD, and LGD subsamples. From the *P*-values in Table 2, we see no statistically significant differences between the radial distributions of SNe in various subsamples. However, when we compare the inner truncated radial distributions ($\tilde{r} \geq 0.2$; shown in brackets), a significant difference appears for CC SNe in LGD versus NGD hosts. The upper panel of Fig. 2 presents the histograms of radii of CC SNe. From these histograms, we see that the radial distribution of CC SNe in NGD subsample is concentrated to the centre of galaxies with a relatively narrow peak and fast decline in the outer disc. In contrast, the distribution of CC SNe in LGD galaxies has a broader peak, shifted to the outer region of the discs, with a somewhat slower decline. The radial distribution of SNe in SGD hosts appears to be intermediate between those in NGD and LGD galaxies.

The inner truncation of the radial distribution of SNe, especially for CC ones, is crucial because of several important effects. The observed numbers of SNe at $\tilde{r} \lesssim 0.2$ indicate that because of high surface brightness of galactic nuclei and imperfect reduction of astronomical images, it is difficult to discover objects at or near the centre of galaxies, even for nearby ones (e.g. Leaman et al. 2011). On the other hand, dust extinction in host galaxy disc, particularly in the nuclear region (e.g. Holwerda et al. 2015), can affect the radial distributions of SNe (e.g. Wang, Höflich & Wheeler 1997; Hatano, Branch & Deaton 1998). Since CC SNe have peak luminosities that are ∼2 magnitudes lower than do SNe Ia (e.g. Richardson et al. 2002), CC SNe are more strongly affected by these effects than are Type Ia SNe.

In Hakobyan et al. (2016), we already demonstrated that in the central regions of unbarred spiral galaxies the surface densities of SNe show a drop, significantly for CC SNe (see also in the middle panel of Fig. 2), in comparison with the exponential surface density profiles of the parent populations (see also van den Bergh 1997; Wang, Deng & Wei 2010). We list, in columns 4 and 5 of Table 3, for different subsamples of the present study, the P_{KS} and P_{AD} probabilities from one-sample KS and AD tests, respectively, that the distributions of SNe are drawn from the best-fitting exponential surface density profiles. We obtain $\Sigma^{SN}(\tilde{r}) = \Sigma_0^{SN} \exp(-\tilde{r}/\tilde{h}_{SN})$ profiles using the maximum likelihood estimation (MLE) method, where $\tilde{h}_{SN}$ is the scale length of the distribution (column 6 of Table 3) and Σ_0^{SN} is the central surface density of SNe. The *P*-values in Table 3 show that the global ($\tilde{r} \geq 0$) distributions of Type Ia SNe in different subsamples are consistent with the exponential profiles. However, the surface density distributions of CC SNe are not consistent with the exponential profiles in all subsamples of host galaxies, except the NGD hosts.

To exclude the selection effects at the centres of host galaxies, we repeat our procedure for $\tilde{r} \geq 0.2$ range (see columns 7–10 in Table 3). Now, with only one exception, the surface density distributions of Type Ia and CC SNe in different subsamples are consistent with the exponential profiles. The inner-truncated scale lengths are in agreement with those in Hakobyan et al. (2016): using nearby low-inclined early-type spiral galaxies (unbarred Sa–Sbc, without splitting the sample according to ACs) we found $\tilde{h}_{SN}^{Ia} = 0.21 \pm 0.03$ and $\tilde{h}_{SN}^{CC} = 0.17 \pm 0.03$ in the SDSS *g*-band.

Only the surface density distribution of CC SNe in LGD galaxies is inconsistent with an inner-truncated exponential profile (as seen in Table 3 for the AD statistic but only very marginally so in the KS statistic). From the middle panel of Fig. 2, we see that the surface density is marginally higher than the best-fitting exponential profile at $0.4 \lesssim \tilde{r} \lesssim 0.7$. The inconsistency becomes more evident if we compare the distribution of CC SNe in LGD galaxies with the inner-truncated exponential profile with the scale length of CC SNe in NGD galaxies ($P_{KS} = 0.005$ and $P_{AD} = 0.001$). For the visualization, the latter (upper blue dashed line in the middle panel of Fig. 2) is also scaled according to the central surface density of the profile in LGD hosts. The bottom panel of Fig. 2 shows the cumulative distributions of CC SN radii with their best-fitting exponential cumulative distribution functions (CDFs).

4 INTERPRETATION WITHIN THE FRAMEWORK OF DENSITY WAVE THEORY

In this section, we interpret the results above in the context of triggered massive star formation by the DWs in GD galaxies, especially

ready commented about the SDSS model failure. Thus, reliable scale lengths are not available for many galaxies of our sample.

[8]The null hypothesis for the two-sample non-parametric KS (or AD) test is that the two distributions being compared are drawn from the same parent population, and the alternative hypothesis that they are not. Traditionally, we chose the threshold of 5 per cent for significance levels (*P*-values) of the tests. The AD test detects differences better than the KS test and generally requires less data to reach sufficient statistical power (Engmann & Cousineau 2011).

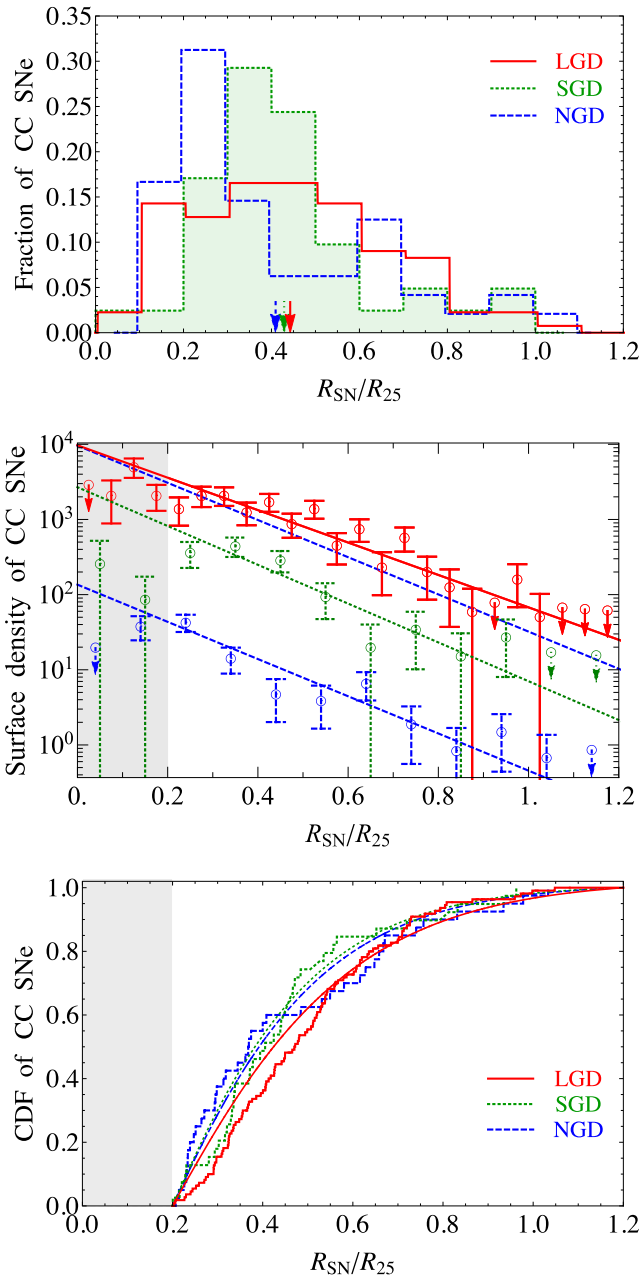

Figure 2. *Upper panel*: distributions of deprojected and normalized galactocentric radii ($\tilde{r} = R_{SN}/R_{25}$) of CC SNe in LGD (red solid), SGD (green dotted), and NGD (blue dashed) host galaxies. The mean values of the distributions are shown by arrows. *Middle panel*: surface density distributions (with arbitrary normalization) of CC SNe in the mentioned hosts. For better visualization, thanks to more data points, the bin size of distribution in LGD galaxies is 0.05, in units of R_{25}, while for the other subsamples the bin size is 0.1. The error bars assume a Poisson distribution. The upper limits of surface density (with +1 SN if none is found) are represented by down arrows. The fitted exponential surface density profiles are estimated for the inner-truncated discs (outside the shaded area). For better visibility, the distributions and profiles are shifted vertically and then sorted by increasing the mean $\tilde{r}$ as one moves upwards, and also slightly shifted horizontally. To visually compare the distribution of CC SNe in LGD hosts with the fitted profile in NGD galaxies, the latter is also positioned with the central surface density matched with that in LGD hosts. *Bottom panel*: inner-truncated cumulative distributions of SN radii and their best-fitting exponential CDFs.

in LGD hosts (e.g. Cepa & Beckman 1990; Seigar & James 2002; Cedrés et al. 2013).

In a simple model of GD host galaxies (Fig. 3), we assume that the spiral pattern rotates with a constant angular velocity, while the gas and stars have differential rotation, and a corotation radius/region (R_C) exists where these two angular velocities are equal. Inside the corotation radius, the disc rotates faster than the spiral arm pattern, and therefore massive star formation triggering is expected in a shock front around the inner edges of arms (thick black curves inside the red solid circle in Fig. 3, see also fig. 9 of Aramyan et al. 2016), as originally proposed by Roberts (1969). On the contrary, outside the corotation radius, the arm pattern rotates faster than the disc. Therefore, gas and stars are caught up by the spiral arms. In this case, star formation is expected to be triggered in a shock front around the outer edges of arms (thick black curves outside red solid circle in Fig. 3). Indeed, in Aramyan et al. (2016), we already showed that the distribution of CC SNe (explosions of young short-lived massive stars) relative to the SDSS *g*-band peaks of spiral arms depends on the galactocentric radial range. In particular, the locations of CC SNe are shifted to the inner and outer edges of the spiral arms inside and outside the mean corotation radius ($\langle R_C/R_{25}\rangle \approx 0.45$) of LGD galaxies, respectively. For Type Ia SNe (explosions of less-massive and longer-lived stars), the distribution relative to spiral arms showed no significant dependence on galactocentric radii.

In the corotation region (thick gray ring in Fig. 3) where the stars and gas rotate at the same velocity as the spiral pattern, the triggering of star formation is not expected, given the absence of spiral shocks. Mainly, the gravitation instability is responsible for the star formation in this region (as in the entire disc of a NGD galaxy). Due to absence of star formation triggering spiral shocks in the corotation region (e.g. Cedrés et al. 2013), the surface density of CC SNe should show a drop around R_C in GD galaxies. At the same time, at large radii ($\gtrsim R_{25}$) the DWs are expected to fade (e.g. Elmegreen et al. 1992). Therefore, at large radii, star formation triggered by shock fronts at the outer edges of arms should be not significant (thick black dashed curves in Fig. 3).

To study the distribution of SNe relative to R_C of hosts, we carried out an extensive literature search for corotation radii of our SGD and LGD galaxies. Only 30 nearby host galaxies ($\lesssim$80 Mpc) with 8 Type Ia and 48 CC SNe have available corotation radii (Table 4). These radii were estimated using different methods. For example, Elmegreen et al. (1992) found clear evidences for the corotation radii in gas-rich galaxies, in the form of sharp endpoints to star formation ridges and dust lanes in GD spirals. Verley et al. (2007) used Fourier analysis and focussed on the modes of the spiral arms, computing the torques between the gas and newly formed stars (Hα emission), and the bulk of the optical matter (*r*-band), which can be used to locate the corotation regions. Buta & Zhang (2009) used the potential-density phase-shift method on deprojected *H*-band images to locate the corotation radii for a large number of spiral galaxies. Font et al. (2014) used the changes in direction of the radial component of the in-plane velocities, using the emission in Hα, at the resonance radii to find corotations in disc galaxies. For more details of these and other methods, the reader is referred to the original papers mentioned in Table 4. Further, in our study, we use these corotation radii normalized to the optical radii of host galaxies in the SDSS *g*-band, i.e. R_C/R_{25}.

In Table 4, it can be seen that for some individual galaxies more than one corotation radius is found. This is not unexpected because real spiral galaxies are more complex physical objects in comparison with the simple model presented in Fig. 3. In some galaxies,

Table 3. Consistency of global ($\tilde{r} \geq 0$) and inner-truncated ($\tilde{r} \geq 0.2$) SN distributions with exponential surface density models in different subsamples of host galaxies.

			$\tilde{r} \geq 0$				$\tilde{r} \geq 0.2$		
Host	SN	N_{SN}	P_{KS}	P_{AD}	$\tilde{h}_{SN}$	N_{SN}	P_{KS}	P_{AD}	$\tilde{h}_{SN}$
(1)	(2)	(3)	(4)	(5)	(6)	(7)	(8)	(9)	(10)
All	Ia	111	0.141	0.148	0.21 ± 0.01	90	0.272	0.333	0.20 ± 0.01
LGD	Ia	61	0.730	0.514	0.22 ± 0.02	50	0.886	0.791	0.20 ± 0.02
SGD	Ia	18	0.318	0.290	0.24 ± 0.03	16	0.737	0.506	0.21 ± 0.03
NGD	Ia	32	0.557	0.489	0.19 ± 0.02	24	0.449	0.379	0.18 ± 0.02
All	CC	222	**0.005**	**0.002**	0.22 ± 0.01	190	0.117	0.172	0.19 ± 0.01
LGD	CC	133	**0.017**	**0.018**	0.22 ± 0.01	111	0.070	**0.043**	0.20 ± 0.01
SGD	CC	41	**0.023**	**0.035**	0.21 ± 0.01	39	0.349	0.440	0.17 ± 0.02
NGD	CC	48	0.191	0.180	0.20 ± 0.02	40	0.579	0.407	0.18 ± 0.02

Notes. Columns 1 and 2 give the subsample; Col. 3 is the number of SNe in the subsample; Cols. 4 and 5 are the P_{KS} and P_{AD} probabilities from one-sample KS and AD tests, respectively, that the global ($\tilde{r} \geq 0$) distribution of SNe is drawn from the best-fitting exponential surface density profile; Col. 6 is the maximum likelihood value of $\tilde{h}_{SN} = h_{SN}/R_{25}$ with bootstrapped error (repeated 10^3 times); Cols. 7–10 are, respectively, the same as Cols. 3–6, but for the inner-truncated ($\tilde{r} \geq 0.2$) distribution. The P_{KS} and P_{AD} are calculated using the calibrations by Massey (1951) and D'Agostino & Stephens (1986), respectively. The statistically significant deviations from an exponential law are highlighted in bold.

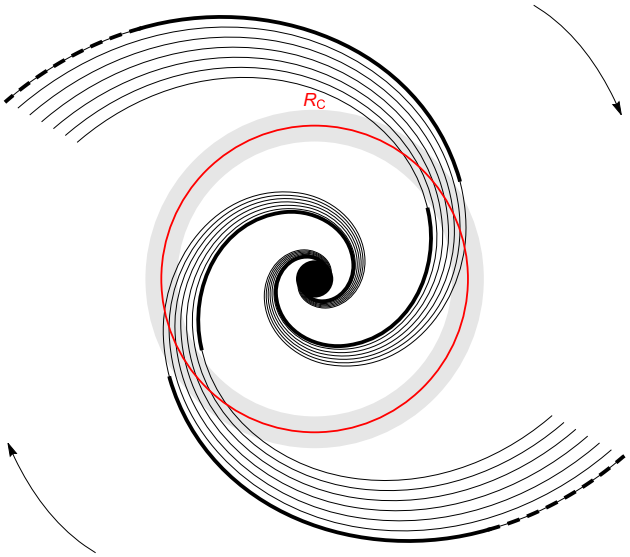

Figure 3. The scheme of massive star formation triggering by DWs in a model of a GD galaxy with two logarithmic spiral arms. The direction of galaxy rotation is illustrated by arrows. The shock fronts of spiral arms are displayed with thick black curves. The corotation region and radius R_C are represented by a thick gray ring and red solid circle, respectively. At large radii ($\gtrsim R_{25}$), the impact of DWs is expected to be weak (shock fronts are presented by thick dashed curves).

single pattern velocities and single corotation radii are observed, while in other systems multiple spiral patterns with different velocities and resonant coupling (e.g. Meidt, Rand & Merrifield 2009), and therefore multiple corotation radii are discovered (e.g. Buta & Zhang 2009; Font et al. 2014). In particular, Buta & Zhang (2009) found that GD galaxies have on average two to three corotation radii, except for exceptionally strong GD spirals (AC = 12), which mostly have a single corotation radius. This is in agreement with our ACs of SNe host galaxies and collected corotation radii in Table 4.

In Fig. 4, we present the galactocentric R_C/R_{25} positions for 30 host galaxies of Table 4, separated according to their ACs: 6 SGD (AC = 5 and 6), 17 LGD (AC = 9), and 7 LGD (AC = 12) galaxies. Here, we separate LGD host galaxies between two ACs in order to check possible differences between the distributions and the mean values of their corotation radii. A similar separation is impossible for SGD galaxies due to the small size of this subsample (see Table 4). In Fig. 4, we also show the galactocentric R_{SN}/R_{25} positions of SNe for each host galaxy.

The mean values of normalized corotation radii and the standard deviations are 0.33 ± 0.16, 0.41 ± 0.18, and 0.46 ± 0.21 for SGD, LGD with AC = 9 and AC = 12 galaxies, respectively. For the united LGD (AC = 9 and 12) subsample, the normalized corotation radius is 0.42 ± 0.18. Meanwhile, the two-sample KS and AD tests show that the difference between the distributions of R_C/R_{25} values in LGD (AC = 9 and 12) and SGD galaxies is statistically not significant ($P_{KS} = 0.550$ and $P_{AD} = 0.312$). The same is valid when comparing the R_C/R_{25} distributions in LGD (AC = 12) and SGD galaxies ($P_{KS} = 0.433$ and $P_{AD} = 0.268$). Therefore, further in our study, we do not separate the LGD subsample. Fig. 5 shows the histograms and cumulative distributions of R_C/R_{25} values of LGD and SGD galaxies. Also, it is important to note that the $\langle R_C/R_{25} \rangle$ value for LGD galaxies is in good agreement with that ($\approx$0.45) adopted in our previous study (Aramyan et al. 2016).

To check the possible impact of DWs on the distribution of SNe (as schematically presented in Fig. 3), we now normalize the SN radii to the corresponding corotation radii of host galaxies. When a host galaxy has two corotation radii in Table 4, we use a proximity criterion, selecting only the value of R_C that is closest to the value of R_{SN}. For LGD host galaxies, Fig. 6 displays the histogram and surface density of 44 CC SNe positions in units of the corotation radii (R_{SN}/R_C). The surface density of CC SNe is consistent with the best-fitting global ($P_{KS} = 0.600$, $P_{AD} = 0.463$) and inner-truncated ($P_{KS} = 0.457$, $P_{AD} = 0.526$) exponential profiles with the MLE scale lengths of $(0.60 \pm 0.04)\, R_C$ and $(0.57 \pm 0.05)\, R_C$, respectively. However, the figure indicates a strong dip at the corotation radius, and excess surface densities of CC SNe at $\simeq 0.8$ and $1.5\, R_C$.

Since the lifetime of massive progenitors of CC SNe is significantly short, their explosion sites, on average, coincide with the birthplace. Therefore, the prominently high surface density of CC SNe in comparison with the best-fitting exponential profile around the mentioned radii, inside and outside the corotation region, can be considered as a plausible indicator of triggered massive star

Table 4. Available corotation radii of our LGD and SGD host galaxies.

Host name (1)	AC (2)	N_{Ia} (3)	N_{CC} (4)	R_C/R_{25} (5)	R_C/R_{25} (6)	References (7)
PGC043118	12	1	0	0.33 ± 0.05		Comerón et al. (2014)
PGC040153	12	1	1	0.30 ± 0.05		Canzian & Allen (1997); Comerón et al. (2014)
PGC038068	12	0	3	0.50 ± 0.08		Rautiainen, Salo & Laurikainen (2008); Buta & Zhang (2009)
PGC030087	12	0	4	0.54 ± 0.13		Tamburro et al. (2008)
PGC024531	12	0	1	0.87 ± 0.11		Verley et al. (2007); Font et al. (2014)
PGC007525	12	0	2	0.30 ± 0.06		Verley et al. (2007)
PGC005974	12	0	3	0.34 ± 0.09		Elmegreen et al. (1992); Egusa et al. (2009); Cedrés et al. (2013)
PGC054018	9	0	1	0.40 ± 0.04		Font et al. (2014)
PGC050063	9	1	3	0.21 ± 0.03	0.45 ± 0.12	Elmegreen et al. (1992); Waller et al. (1997); Cedrés et al. (2013)
PGC042833	9	0	2	0.37 ± 0.04	0.57 ± 0.05	Buta & Zhang (2009); Font et al. (2014)
PGC039578	9	0	4	0.34 ± 0.06	0.57 ± 0.07	Elmegreen et al. (1992); Gonzalez & Graham (1996); Buta & Zhang (2009)
PGC038618	9	0	1	0.30 ± 0.01	0.54 ± 0.06	Buta & Zhang (2009)
PGC037845	9	0	1	0.21 ± 0.06	0.40 ± 0.06	Buta & Zhang (2009)
PGC037229	9	0	4	0.46 ± 0.08		Elmegreen et al. (1992); Buta & Zhang (2009)
PGC036789	9	0	1	0.22 ± 0.06		Comerón et al. (2014)
PGC036243	9	0	2	0.45 ± 0.13		Kranz, Slyz & Rix (2003); Buta & Zhang (2009)
PGC034767	9	0	3	0.28 ± 0.03		Fridman et al. (2001)
PGC032614	9	0	2	0.69 ± 0.02	0.83 ± 0.04	Font et al. (2014)
PGC031968	9	0	1	0.26 ± 0.02		Font et al. (2014)
PGC027074	9	0	1	0.30 ± 0.06		Comerón et al. (2014)
PGC024111	9	1	1	0.65 ± 0.06		Comerón et al. (2014)
PGC022279	9	0	1	0.16 ± 0.06		Verley et al. (2007)
PGC002246	9	0	1	0.14 ± 0.06	0.57 ± 0.06	Verley et al. (2007)
PGC002081	9	0	1	0.38 ± 0.05		Elmegreen et al. (1992); Sempere & Rozas (1997)
PGC038031	6	1	0	0.22 ± 0.03	0.42 ± 0.02	Font et al. (2014); Comerón et al. (2014)
PGC027723	6	1	0	0.17 ± 0.06	0.44 ± 0.06	Comerón et al. (2014)
PGC012626	6	2	0	0.48 ± 0.03		Buta & Zhang (2009)
PGC035594	5	0	1	0.32 ± 0.06		Font et al. (2014)
PGC034836	5	0	2	0.12 ± 0.06	0.58 ± 0.06	Buta & Zhang (2009)
PGC030010	5	0	1	0.17 ± 0.06	0.41 ± 0.06	Comerón et al. (2014)

Notes. Column 1 is the host galaxy PGC name; Col. 2 is the galaxy AC (see SubSection 2.2); Cols. 3 and 4 are the numbers of Type Ia and CC SNe in the galaxy; Cols. 5 and 6 are the normalized corotation radii of the galaxy; Col. 7 represents the references of corotation radii. The R_C/R_{25} values are calculated using the R_C in arcsec from the mentioned references and the galaxy R_{25} in the SDSS *g*-band (see SubSection 2.1). When more than one references are available for the same corotation region and the reported radii are matched within the errors, we list their mean values. Nuclear and circumnuclear corotation radii (coincided with star-forming rings/ovals), as well as those with uncertain (very weak/noisy) estimation are not selected from the references.

formation by the DWs in LGD host galaxies. These results are in agreement with those of Cedrés et al. (2013), who found clear evidence of massive star formation triggering in the sense of a high density of H II regions at the fixed radii, avoiding the corotation region, created after the passage of the arm material through the DW in some GD galaxies (see also Cepa & Beckman 1990; Seigar & James 2002).

Considering that the different LGD host galaxies have various corotation radii (see Table 4 and Fig. 4) distributed around the mean value of $\langle R_C/R_{25}\rangle = 0.42 \pm 0.18$ (see Fig. 5), the radii of triggered star formation by DWs should be blurred within a radial region including ∼0.4 to ∼0.7 range in units of R_{25}, preventing to observe a drop in the mean corotation region (middle panel of Fig. 2). Therefore, most probably, the impact of DWs (triggering effect) is responsible for a marginally higher surface density of CC SNe within the mentioned radial range, and for the inconsistency of the surface density distribution with the inner-truncated exponential profile in LGD hosts (middle panel of Fig. 2 and Table 3).

To check the significance of the drop of surface density at R_C and excess at ≃0.8 and 1.5 R_C (see Fig. 6), we study the distribution of CC SNe distances to the nearest corotation in units of corotation radius, $D = |R_{SN} - R_C|/R_C$. Fig. 7 displays the differential and cumulative distances in the global disc of LGD galaxies. Since a given value of distance can occur either for position $1 - D$ or for position $1 + D$ (both in units of corotation radius), the probability distribution function (PDF) of distances follows

$$\mathrm{PDF}(D) = \begin{cases} f(1-D) + f(1+D), & 0 < D \leq 1 \\ f(1+D), & D > 1 \end{cases} \quad (1)$$

$$f(x) = \frac{x}{h^2}\,\exp(-\frac{x}{h})\,, \quad (2)$$

where h is the best-fitting scale length of the SNe (in units of the corotation radii). The CDF for D is then

$$\mathrm{CDF}(D) = \begin{cases} g(1-D) - g(1+D), & 0 < D \leq 1 \\ 1 - g(1+D), & D > 1 \end{cases} \quad (3)$$

$$g(x) = \left(1 + \frac{x}{h}\right)\,\exp\left(-\frac{x}{h}\right). \quad (4)$$

In Fig. 7, the black curves are the best-fitting (with MLE) expected distribution. Fig. 7 highlights the lack of CC SNe at corotation and excess outside/inside the R_C in the LGD hosts. However, a KS test indicates a *P*-value of 0.176, while an AD test indicates a *P*-value of 0.197. We check the significance of the drop/excess in the global disc, adding also four CC SNe from SGD sample. The result is: $P_{KS} = 0.170$ and $P_{AD} = 0.224$. For the inner-truncated disc of LGD (LGD+SGD) galaxies, the $P_{KS} = 0.353\,(0.445)$ and

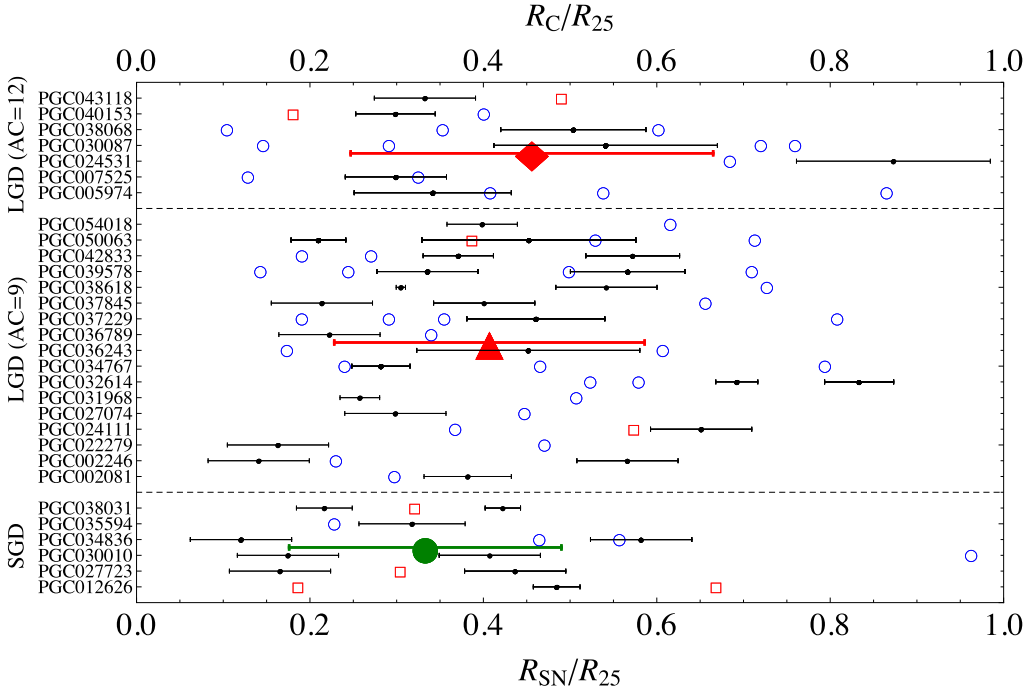

Figure 4. Galactocentric positions of normalized corotation radii (black points) and their errors for 30 host galaxies of Table 4. SGD (AC = 5 and 6), LGD (AC = 9), and LGD (AC = 12) galaxies are separated by horizontal dashed lines. The filled diamond, triangle, and circle are the corresponding mean values of the corotation radii (with their standard deviations). For each host galaxy, galactocentric positions of Type Ia (red empty squares) and CC (blue empty circles) SNe are also presented. In PGC 050063, one of the CC SNe is located at $R_{SN}/R_{25} = 1.59$ and not shown in the plot.

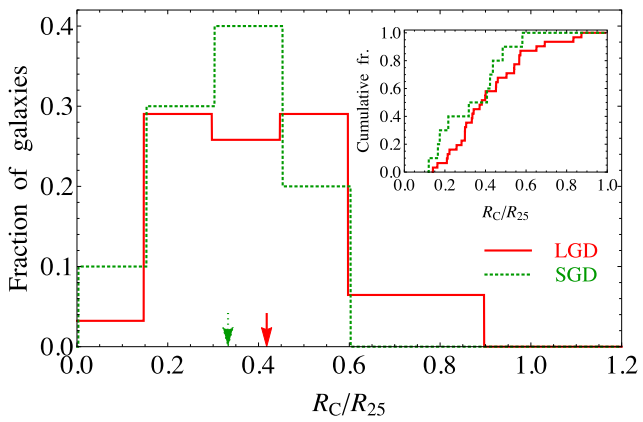

Figure 5. Histograms and cumulative distributions (inset) of R_C/R_{25} values of LGD (red solid) and SGD (green dotted) galaxies. The mean values are shown by arrows.

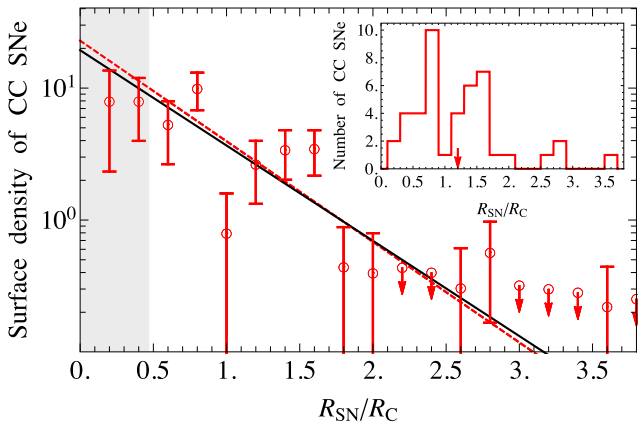

Figure 6. Surface density profile of CC SNe (with arbitrary normalization) in LGD host galaxies. The error bars assume a Poisson distribution. The upper limits of surface density (with +1 SN if none is found) are represented by down arrows. The black solid and red dashed lines are the best maximum-likelihood fits of global and inner-truncated (from 0.48 corotation radii outwards to avoid the obscured inner region [grey shaded]) exponential surface density models, respectively. The inset presents the histogram of SN radii (the mean value is shown by arrow).

$P_{AD} = 0.299$ (0.428). Thus, the lack of CC SNe at corotation and excess at $\simeq$0.8 and 1.5 R_C do not appear statistically significant. Note that these tests ignore the uncertainties on the corotation radii. Including them would weaken even more the statistical significance of these features in the surface density profile of CC SNe.

It is important to note that, if one wants to test the star formation activity at the corotation, the estimates of corotation radii based on kinematic or dynamic arguments (e.g. Font et al. 2014) would be preferable as they would be more independent of the regions with lack of star formation (e.g. Elmegreen et al. 1992) or specific morphological features in the discs (e.g. Buta & Zhang 2009). Only 18 CC SNe (17 in LGD and one in SGD) have host galaxies with such preferable estimates of R_C. If we consider only these objects, the triggering evidence and the dip in the global disc remain not significant ($P_{KS} = 0.514$ and $P_{AD} = 0.425$), probably due to even smaller statistics.

Another importance is that galaxies with several spiral patterns with different angular velocities, i.e. more than one corotation, might have interactions between the patterns (e.g. Font et al. 2014, at R_C of one with inner/outer Lindblad resonance of the other) causing turbulence in the interface regions between the patterns and thereby

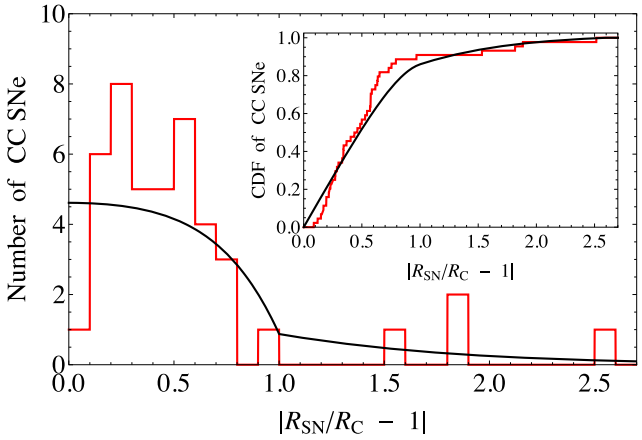

Figure 7. Differential distribution of the distances of CC SNe to nearest corotation radius in the global disc of LGD galaxies (normalized to the corotation radius). The inset presents the CDF of the distances. The black curves indicate the distribution of normalized distances to corotation expected for the best-fitting exponential surface density model (scale length of 0.60 R_C), using equations (1), (2), (3), and (4).

increase star formation activity at those regions (see reviews by Dobbs & Baba 2014; Shu 2016). Therefore, the distribution of CC SNe (Figs. 6 and 7) might be contaminated by the objects at the R_C, weakening the observed dip. In Table 4, we see that 31 CC SNe (30 in LGD and one in SGD) have host galaxies with single R_C. If we consider only these objects, the triggering evidence and the dip in the global disc are again statistically not significant ($P_{KS} = 0.457$ and $P_{AD} = 0.354$).

Unfortunately, due to the insufficient number of CC SNe in SGD galaxies (only 4 objects, see Table 4), as well as Type Ia SNe in the LGD (4 cases) and SGD (4 objects) subsamples, a similar study of their distributions relative to R_C is ineffective. In the future, when more information is available on corotation radii of SN host galaxies, we will be able to extend our study including all SN types in LGD and SGD galaxies.

5 CONCLUSIONS

In this study, using a well-defined and homogeneous sample of SN host galaxies from the coverage of SDSS DR13, we analyse the radial and surface density distributions of Type Ia and CC SNe in host galaxies with different ACs to find the possible impact of spiral DWs as triggers for star formation. Our sample consists of 269 relatively nearby ($\leq$150 Mpc, the mean distance is 82 Mpc), low-inclination ($i \leq 60^\circ$), morphologically non-disturbed and unbarred Sa–Sc galaxies, hosting 333 SNe in total. In addition, we perform an extensive literature search for corotation radii, collecting data for 30 host galaxies with 56 SNe.

The main results concerning the deprojected and inner-truncated ($\tilde{r} \geq 0.2$) distributions of SNe in host galactic discs are the following:

(i) We find no statistical differences between the pairs of the R_{25}-normalized radial distributions of Type Ia and CC SNe in discs of host galaxies with different spiral ACs, with only one significant exception: CC SNe in LGD and NGD galaxies have significantly different radius distributions (Table 2). The radial distribution of CC SNe in NGDs is concentrated to the centre of galaxies with relatively narrow peak and fast exponential decline at the outer region, while the distribution of CC SNe in LGD galaxies has a broader peak, shifted to the outer region of the discs (upper panel of Fig. 2).

(ii) The surface density distributions of Type Ia and CC SNe in most of the subsamples are consistent with the exponential profiles. Only the distribution of CC SNe in LGD galaxies appears to be inconsistent with an exponential profile (Table 3 for the AD statistic but only very marginally so for the KS statistic), being marginally higher at $0.4 \lesssim R_{SN}/R_{25} \lesssim 0.7$. The inconsistency becomes more evident when comparing the same distribution with the scaled exponential profile of CC SNe in NGD galaxies (middle panel of Fig. 2).

(iii) Using a smaller sample of LGD galaxies with estimated corotation radii, we show, for the first time, that the surface density distribution of CC SNe shows a dip at corotation, and enhancements at $^{+0.5}_{-0.2}$ corotation radii around it (Fig. 6). However, these features are not statistically significant (Fig. 7). The CC SNe enhancements around corotation may, if confirmed with larger samples, indicate that massive star formation is triggered by the DWs in LGD host galaxies. Considering that the different LGD host galaxies have various corotation radii (Table 4 and Fig. 4) distributed around the mean value of $\langle R_C/R_{25} \rangle = 0.42 \pm 0.18$ (Fig. 5), the radii of triggered star formation by DWs are most probably blurred within a radial region including ~0.4 to ~0.7 range in units of R_{25}, without a prominent drop in the mean corotation region (middle panel of Fig. 2).

These results for CC SNe in LGD galaxies may, if confirmed with larger samples and better corotation estimates, support the large-scale shock scenario (e.g. Moore 1973), originally proposed by Roberts (1969), which predicts a higher star formation efficiency, avoiding the corotation region (e.g. Cepa & Beckman 1990; Seigar & James 2002; Cedrés et al. 2013; Aramyan et al. 2016).

When more information will become available on corotation radii of SN host galaxies, it would be worthwhile to extend our study, by comparing the R_C-normalized radial and surface density distributions of Type Ia and CC SNe in LGD galaxies. This will also allow to check the impact of spiral DWs on the distribution of less-massive and longer-lived progenitors of Type Ia SNe. Moreover, similar analysis of SNe in SGD galaxies can help to understand the role of DWs in star formation triggering, if any.

ACKNOWLEDGEMENTS

We would like to thank the referee, Preben Grosbøl, for excellent comments that improved the clarity of this paper. AGK, AAH, and LVB acknowledge the hospitality of the Institut d'Astrophysique de Paris (France) during their stay as visiting scientists supported by the Programme Visiteurs Extérieurs (PVE). This work was supported by the RA MES State Committee of Science, in the frames of the research project number 15T–1C129. This work was made possible in part by a research grant from the Armenian National Science and Education Fund (ANSEF) based in New York, USA. V.A. acknowledges the support from Fundação para a Ciência e Tecnologia (FCT) through Investigador FCT contract nr. IF/00849/2015/CP1273/CT0003 and the support from FCT through national funds and by FEDER through COMPETE2020 by the grant PTDC/FIS-AST/7073/2014 & POCI-01-0145-FEDER-016880. Funding for the SDSS-IV has been provided by the Alfred P. Sloan Foundation, the US Department of Energy Office of Science, and the Participating Institutions. SDSS-IV acknowledges support and resources from the Center for High-Performance Computing at the University of Utah. The SDSS web site is

www.sdss.org. SDSS–IV is managed by the Astrophysical Research Consortium for the Participating Institutions of the SDSS Collaboration including the Brazilian Participation Group, the Carnegie Institution for Science, Carnegie Mellon University, the Chilean Participation Group, the French Participation Group, Harvard-Smithsonian Center for Astrophysics, Instituto de Astrofísica de Canarias, The Johns Hopkins University, Kavli Institute for the Physics and Mathematics of the Universe (IPMU) University of Tokyo, Lawrence Berkeley National Laboratory, Leibniz Institut für Astrophysik Potsdam (AIP), Max-Planck-Institut für Astronomie (MPIA Heidelberg), Max-Planck-Institut für Astrophysik (MPA Garching), Max-Planck-Institut für Extraterrestrische Physik (MPE), National Astronomical Observatories of China, New Mexico State University, New York University, University of Notre Dame, Observatário Nacional / MCTI, The Ohio State University, Pennsylvania State University, Shanghai Astronomical Observatory, United Kingdom Participation Group, Universidad Nacional Autónoma de México, University of Arizona, University of Colorado Boulder, University of Oxford, University of Portsmouth, University of Utah, University of Virginia, University of Washington, University of Wisconsin, Vanderbilt University, and Yale University.

REFERENCES

Albareti F. D. et al., 2017, ApJS, 233, 25
Anderson J. P., James P. A., Habergham S. M., Galbany L., Kuncarayakti H., 2015, PASA, 32, e019
Ann H. B., Lee H.-R., 2013, J. Kor. Astron. Soc., 46, 141
Aramyan L. S. et al., 2016, MNRAS, 459, 3130
Barbon R., Buondí V., Cappellaro E., Turatto M., 1999, A&AS, 139, 531
Bartunov O. S., Tsvetkov D. Y., Filimonova I. V., 1994, PASP, 106, 1276
Bittner A., Gadotti D. A., Elmegreen B. G., Athanassoula E., Elmegreen D. M., Bosma A., Muñoz-Mateos J.-C., 2017, MNRAS, 471, 1070
Bottinelli L., Gouguenheim L., Paturel G., Teerikorpi P., 1995, A&A, 296, 64
Buta R. J., 2013, in Oswalt T. D., Keel W. C., eds, Planets, Stars and Stellar Systems, Vol. 6: Extragalactic Astronomy and Cosmology. Springer, Dordrecht, p. 1
Buta R. J., Zhang X., 2009, ApJS, 182, 559
Buta R. J. et al., 2015, ApJS, 217, 32
Canzian B., Allen R. J., 1997, ApJ, 479, 723
Cappellaro E., Turatto M., 1997, in Ruiz-Lapuente P., Canal R., Isern J., eds, NATO Adv. Sci. Inst. Ser. C, Vol. 486, Thermonuclear Supernovae. Springer, Dordrecht, p. 77
Cedrés B., Cepa J., Bongiovanni Á., Castañeda H., Sánchez-Portal M., Tomita A., 2013, A&A, 560, A59
Cepa J., Beckman J. E., 1990, ApJ, 349, 497
Comerón S. et al., 2014, A&A, 562, A121
D'Agostino R. B., Stephens M. A., 1986, Goodness-of-Fit Techniques, Statistics: Textbooks and Monographs, Vol. 68, Marcel Dekker Inc., New York, Basel
Dobbs C., Baba J., 2014, PASA, 31, e035
Egusa F., Kohno K., Sofue Y., Nakanishi H., Komugi S., 2009, ApJ, 697, 1870
Elmegreen D. M., Elmegreen B. G., 1987, ApJ, 314, 3
Elmegreen B. G., Elmegreen D. M., Montenegro L., 1992, ApJS, 79, 37
Engmann S., Cousineau D., 2011, J. Appl. Quant. Methods, 6, 1
Font J., Beckman J. E., Querejeta M., Epinat B., James P. A., Blasco-herrera J., Erroz-Ferrer S., Pérez I., 2014, ApJS, 210, 2
Foyle K., Rix H.-W., Walter F., Leroy A. K., 2010, ApJ, 725, 534
Fridman A. M. et al., 2001, MNRAS, 323, 651
Gerola H., Seiden P. E., 1978, ApJ, 223, 129
Gonzalez R. A., Graham J. R., 1996, ApJ, 460, 651
Grosbøl P., Dottori H., 2009, A&A, 499, L21
Grosbøl P., Dottori H., 2012, A&A, 542, A39
Habergham S. M., Anderson J. P., James P. A., Lyman J. D., 2014, MNRAS, 441, 2230
Hakobyan A. A., Mamon G. A., Petrosian A. R., Kunth D., Turatto M., 2009, A&A, 508, 1259
Hakobyan A. A., Adibekyan V. Z., Aramyan L. S., Petrosian A. R., Gomes J. M., Mamon G. A., Kunth D., Turatto M., 2012, A&A, 544, A81
Hakobyan A. A. et al., 2014, MNRAS, 444, 2428
Hakobyan A. A. et al., 2016, MNRAS, 456, 2848
Hakobyan A. A. et al., 2017, MNRAS, 471, 1390
Hatano K., Branch D., Deaton J., 1998, ApJ, 502, 177
Holwerda B. W., Reynolds A., Smith M., Kraan-Korteweg R. C., 2015, MNRAS, 446, 3768
James P. A., Percival S. M., 2018, MNRAS, 474, 3101
James P. A., Bretherton C. F., Knapen J. H., 2009, A&A, 501, 207
Knapen J. H., Beckman J. E., Cepa J., Nakai N., 1996, A&A, 308, 27
Kranz T., Slyz A., Rix H.-W., 2003, ApJ, 586, 143
Leaman J., Li W., Chornock R., Filippenko A. V., 2011, MNRAS, 412, 1419
Lin C. C., Shu F. H., 1964, ApJ, 140, 646
Maoz D., Mannucci F., 2012, PASA, 29, 447
Martínez-García E. E., González-López lira R. A., Bruzual-A G., 2009, ApJ, 694, 512
Massey F. J., 1951, J. Am. Stat. Assoc., 46, 68
Maund J. R., 2018, MNRAS, 476, 2629
Maza J., van den Bergh S., 1976, ApJ, 204, 519
McCall M. L., Schmidt F. H., 1986, ApJ, 311, 548
McMillan R. J., Ciardullo R., 1996, ApJ, 473, 707
Meidt S. E., Rand R. J., Merrifield M. R., 2009, ApJ, 702, 277
Mikhailova G. A., Bartunov O. S., Tsvetkov D. Y., 2007, Astron. Lett., 33, 715
Moore E., 1973, PASP, 85, 564
Mueller M. W., Arnett W. D., 1976, ApJ, 210, 670
Pastorello A. et al., 2018, MNRAS, 474, 197
Paturel G. et al., 1997, A&AS, 124, 109
Petrosian A. et al., 2005, AJ, 129, 1369
Pettitt A. N., 1976, Biometrika, 63, 161
Pour-Imani H., Kennefick D., Kennefick J., Davis B. L., Shields D. W., Shameer Abdeen M., 2016, ApJ, 827, L2
Rautiainen P., Salo H., Laurikainen E., 2008, MNRAS, 388, 1803
Richardson D., Branch D., Casebeer D., Millard J., Thomas R. C., Baron E., 2002, AJ, 123, 745
Roberts W. W., 1969, ApJ, 158, 123
Schlegel D. J., Finkbeiner D. P., Davis M., 1998, ApJ, 500, 525
Seigar M. S., James P. A., 2002, MNRAS, 337, 1113
Sellwood J. A., 2011, MNRAS, 410, 1637
Sempere M. J., Rozas M., 1997, A&A, 317, 405
Shabani F. et al., 2018, MNRAS, 478, 3590
Shu F. H., 2016, ARA&A, 54, 667
Silverman J. M. et al., 2013, ApJS, 207, 3
Smith N., Li W., Filippenko A. V., Chornock R., 2011, MNRAS, 412, 1522
Spergel D. N. et al., 2007, ApJS, 170, 377
Tamburro D., Rix H.-W., Walter F., Brinks E., de Blok W. J. G., Kennicutt R. C., Mac Low M.-M., 2008, AJ, 136, 2872
van den Bergh S., 1997, AJ, 113, 197
Verley S., Combes F., Verdes-Montenegro L., Bergond G., Leon S., 2007, A&A, 474, 43
Waller W. H. et al., 1997, ApJ, 481, 169
Wang L., Höflich P., Wheeler J. C., 1997, ApJ, 483, L29
Wang J., Deng J. S., Wei J. Y., 2010, MNRAS, 405, 2529
Williams B. F., Hillis T. J., Murphy J. W., Gilbert K., Dalcanton J. J., Dolphin A. E., 2018, ApJ, 860, 39
Xiao L., Galbany L., Eldridge J. J., Stanway E. R., 2018, preprint (arXiv: 1805.01213)

SUPPORTING INFORMATION

Supplementary data are available at *MNRAS* online.

Please note: Oxford University Press is not responsible for the content or functionality of any supporting materials supplied by the authors. Any queries (other than missing material) should be directed to the corresponding author for the article.

This paper has been typeset from a TEX/LATEX file prepared by the author.